Visualizing Unsteady Vortical Behavior of a Centrifugal Pump

Mathias Otto
University of Magdeburg

Alexander Kuhn
University of Magdeburg

Wito Engelke
University of Magdeburg / KAUST

Holger Theisel
University of Magdeburg

Abstract

In this work we are going to present our results analyzing a centrifugal pump as a part of the IEEE Visualization Contest 2011. The given data set represents a high resolution simulation of a centrifugal pump operating below optimal speed settings. Our goal is to find suitable visualization techniques to identify areas of recirculation that impede the effectiveness of the pump in practical application. We split our analysis into three parts based on the functional behavior of the pump and applied a set of local and integration based techniques to communicate the unsteady flow behavior in different regions of the data set. Based on this we will present a direct comparison of a set of common vortex extractors and more recent approaches and discuss their applicability. Further, we will show that integration based methods (e.g. separation measures, accumulated scalar fields, particle path lines, and advection textures) are well suited to capture the complex time-dependent behavior of the flow within the given time interval.

1 Introduction

Basing on the dataset information given on the accompanying website[1] we prepared an in depth analysis of the presented data set which will be presented in this paper. The given data represents a high resolution simulation of a centrifugal pump used to transport liquids within pipe systems with a broad range of practical applications. A detailed overview of the simulation settings and physical context is described by Lucius et al. [1]. The main components of this device can be split into a inlet area, an moving impeller producing a rotatory motion within the flow, and an area where the accelerated liquid is finally transported into the outlet areas. This functional principal is illustrated in figure 1. Based on this scheme we focused our study on three major aspects of the device: First, we analyzed the behavior of the incoming flow within the inlet area and its transport into the rotatory impeller area in section 2.2. Second, we observed the general flow behavior by means of fluid transport in those areas where the liquid forced into rotatory motion by the blade of the moving impeller (see section 2.3). Finally, we take a general look on the comparison of the turbulence models throughout all provided simulation models within section 3. We will especially focus on the SAS model, as it will be shown to have the most complex turbulence model and is assumed to be closest to the real flow processes. Still, for most of our integration based models we will provide a comparative overview of the results. For each tasks we derive implications to the functional principle described above. We integrated the given information by the additional pressure scalar field to backup the findings of our velocity field analysis (figure 5). In order to answer these questions, a set of specific visualization methods tailored towards presenting functional relations between different transport effects have been utilized. More details about the used software and visualization tools are presented in section 4.

[1] http://viscontest.sdsc.edu/2011/

2 Data Set Analysis

The given data set was available in Ensight ASCII and Ansys format, including two velocity fields, four common scalar fields and up to three additional method specific fields describing turbulence parameters of the respective simulation models. The fields were given as a vertex based description on a adaptive hexahedral volume grid containing 6.7 Million nodes and 6.5 Million cells. The data contains one complete circulation of the rotor sampled in 80 time steps taken from a longer simulation run. Note, that due to the strong differences in between the first and last time steps an non-periodic flow behavior is assumed for the given time interval.

2.1 Functional Behavior

Based on its practical task the given centrifugal pump can be split into specific regions of different functionality during the running state. The first inlet region guides the flow in orthogonal angle to the rotor area. The rotating impeller accelerates the incoming fluid and enforces a rotatory motion adding kinetic energy while increasing the pressure (see figure 2) due to centrifugal forces. In this case, the impeller consists of five rotatory blades that divide the inflow into five different channels. Note, that we will use an fixed clockwise enumeration scheme for the individual channels shown in the first image in figure 9 and a constant x, y perspective for all images of the transport section. During movement, the impeller distributes the incoming fluid among those channels and accelerates the flow outwards into the diffuser area. Within this area the flow travels at high speed on circular path lines towards the outlet geometry. This behavior is illustrated in figure 7 and 8. The overall goal is to optimize the flow throughput of the incoming fluid. In general this implicates that recirculation areas which are mostly correlated to vortex structures within the channels and the in- and outflow areas are sought to be avoided. Thus, our analyzes focuses on the identification and analysis of vortical transport structures within those functionally important regions and correlates them with features that appear in the scalar fields.

2.2 Inlet Behavior

The pumping device is characterized by a substantial pressure increase while observing the motion towards the outflow region (see figure 2, first row). Minima in the local pressure values are known to correlate to centers of rotatory flow motion. Due to the strong gradient in the pressure function, those minima are difficult to identify in this case. Although they provide information about local pressure minima (e.g. in channel 2 in figure 2 top row), they do not provide information about the overall impact of those features regarding functional aspects. Considering the flow behavior in the **inlet area**, the distribution into the channels is nearly equal. However, having a closer look at the inlet boundary reveals a backward moving flow close to the boundary of the system. This becomes visible looking at the path lines seeded between inlet and transport region as shown in figure 8. The reasons for this can be seen in the pressure compensation within the small back flow channel above the rotor and the inadequate outflow rate of the overall device.

2.3 Transport Behavior

The **transport area** connects the inlet to the diffuser area of the device. In this part two major processes dominate the functionality

of the machine: First, a distribution of the incoming flow among all impeller sections. Second, the transport of the flow out of the channels into the diffuser area. In the assumed ideal case both distribution processes should be rotationally-symmetric and have equal volume fractions among all channels. As the give pump operates below optimal velocities this induces the creation of vortices and subsequently dominant recirculation areas. Those areas are of special interest as they directly decrease the efficiency of the machine and lead to an asymmetric load balance among all blades.

Looking at figure 2 it becomes obvious that from the local scalar fields no direct conclusions about the longterm flow behavior can be drawn. Thus, we utilized a set of approaches to extract local vortex core regions. We applied those methods to the SAS simulation model, as it is assumed to be the model with the most complex turbulence behavior. Two popular methods to extract vortex regions are the λ_2 criterion [4] and the Q-Criterion [5]. The results are shown in figure 3 in the first two rows and in figure 4 as 3D isosurface plots. In addition to this we applied the more recent vortex criteria proposed by Sujudi and Haimes [6] to gain additional insight into the structure of the vortical regions and compare the results given by different vortex definitions. As one approach to capture the time-dependent vortex behavior we applied the swirling cores detector proposed by Weinkauf et al. [7]. Both results are show in the last two rows in figure 3. Note, that both criteria are extracted using a parallel vectors definition that only give a binary information about vortex locations that can be extracted as line structures in a additional post-processing step. The application of those local definitions reveal significant differences in the areas and locations of strong recirculation zones. While the Q and λ_2 criteria extract a large amount of vortical regions in every time step, more specific locations can be identified using Sujudi and Haimes and swirling cores. Still, neither a direct statement about blocked channels can be made nor a more global quantification of vortex areas is provided. In addition to this, an advanced and physically motivated overview about a variety of measures including a global frequency analysis is presented by Lucius et al. [2].

As indicated by the application of the local methods in this case the long term behavior of the flow is of special importance. This can be evaluated by using integration based or Lagrangian methods that observe the global unsteady flow behavior over a given time interval. One method of observing the separational flow behavior are Lagrangian Coherent Structures (LCS). A common definition for visualizing LCS are Finite-Time Lyapunov Exponent (FTLE) [3]. Locally high values in the resulting field represent areas of high particle separation, while local minima may indicate vortex core regions as shown in figure 6. The temporal evolution of such features is shown in the video using a short range integration of $t_d = 20$ moving over the complete time frame. In combination with this separation analysis we applied a texture advection method to reveal the transport behavior among the different channels of the data set. Using the given velocities we integrate the regional information encoded in a predefined volume texture to obtain a quantitative statement about the flow distribution among the channels, potential blocking and recirculation effects (see figure 9). In addition to the aforementioned methods we observed the integral behavior of the given scalar quantities along time-dependent particle traces. A direct indicator of the longterm differences between flow regions is the arc length of the resulting path lines. It reveals flow separations structures and path lines remaining close to the center of vortex regions which is illustrated in figure 11. Further, we accumulated the given pressure along the path lines resulting in a description of its longterm behavior during the circulation (see figure 5). Note, that all scalar fields for the Lagrangian methods are computed in the relative velocity frame (for FTLE the absolute frame would lead to the same results).

3 Simulation Model Comparison

With the data set three different simulation models where given to assess the behavior of the flow (namely SAS, DES, SST). The main difference between those models is the modeling of turbulence. In order to illustrate differences we applied out aforementioned integration based methods to all three simulation models. Longer integration times directly reflect the degree and effect of turbulence over the considered time interval in the resulting scalar fields. All Lagrangian methods reveal a significantly more complex turbulence behavior for the SAS model. Additionally, the blocking of individual channels and the components of specific vortex areas cannot be observed in the DES and SST model. A comparison of all models is presented in the accompanying video.

4 Implementation

To obtain our results we implemented a prototypic software to convert, load and process the given data. We use a notebook with an Intel I7 2820QM (8 cores) and 16 GB RAM as test system. The first step to handle the large amount of data was the conversion from ASCII to binary Ensight format (only 22.2 GB per model instead of 142 GB). Our C# prototype is accelerated by the Task Parallel Library which easily distributes all computations to multiple cores of one computer. The program loads all time steps of one vector data set and one scalar data set of one model. For the interpolation inside the hexahedral cells we use the Mean-Value Coordinate method equivalent to the one used in the ParaView Toolkit. The integration within the velocity fields is done using a lower order Runge-Kutta scheme. Slices of local measures like Q, λ_2, Sujudi Haimes and Swirling Cores are computed in real time. Computations of these measures over the whole volume take about one minute. Integration based methods seeded at all vertices of the whole volume take about one minute per step. However, the resolution of the given gird is much to coarse to represent the delicate structures produced by these methods. For this reason, we compute integration based methods on slices with dense uniform distributed seeds of path lines. In addition to our tool we visualize our results using the commercial visualization packages EnSight CFD[2] and the open-source tool ParaView[3].

Acknowledgements

The project SemSeg acknowledges the financial support of the Future and Emerging Technologies (FET) programme within the Seventh Framework Program for Research of the European Commission, under FET-Open grant number 226042.

References

[1] G. A. Lucius. Unsteady cfd simulations of a pump in part load conditions using scale-adaptive simulation. *International Journal of Heat and Fluid Flow*, 31:1113–1118, 2010.

[2] G. A. Lucius. Numerical simulation and evaluation of velocity fluctuations during rotating stall of a centrifugal pump. *Journal of Fluids Engineering*, 133:081102, 2011.

[3] G. Haller. Lagrangian coherent structures and the rate of strain in two-dimensional turbulence. *Phys. Fluids*, 30(13):3365–3385, 2001.

[4] G. Haller. An objective definition of a vortex. *Journal of Fluid Mechanics*, 525:1–26, Feb. 2005.

[5] J. Jeong. On the identification of a vortex. *Journal of Fluid Mechanics*, 285:69–94, 1995.

[6] D. Sujudi and R. Haimes. Identification of swirling flow in 3D vector fields. Technical report, Department of Aeronautics and Astronautics, MIT, 1995.

[7] T. Weinkauf, J. Sahner, H. Theisel, H.-C. Hege, and S. H.-P. Cores of swirling particle motion in unsteady flows. *IEEE Transactions on Visualization and Computer Graphics*, 13(6):1759–1766, 2007.

[2] http://www.ensightcfd.com/

[3] http://www.paraview.org/

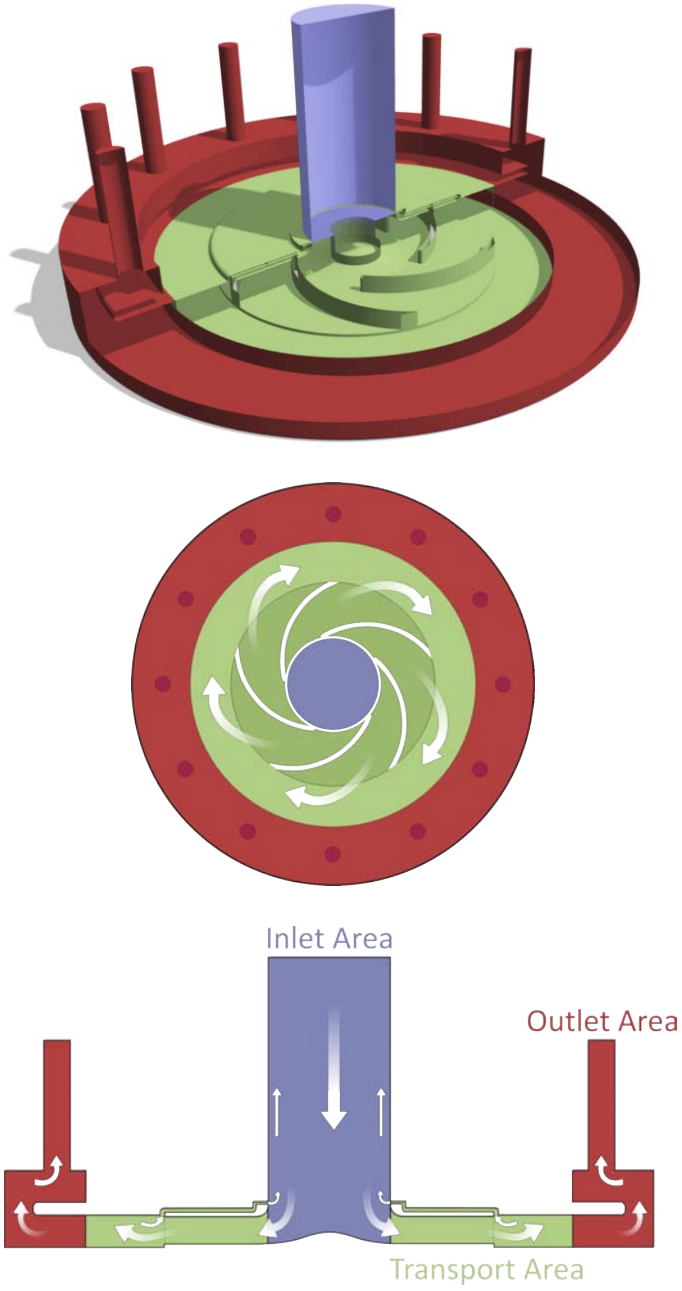

Figure 1: Functional overview of the pump and sectioning based on transport behavior.

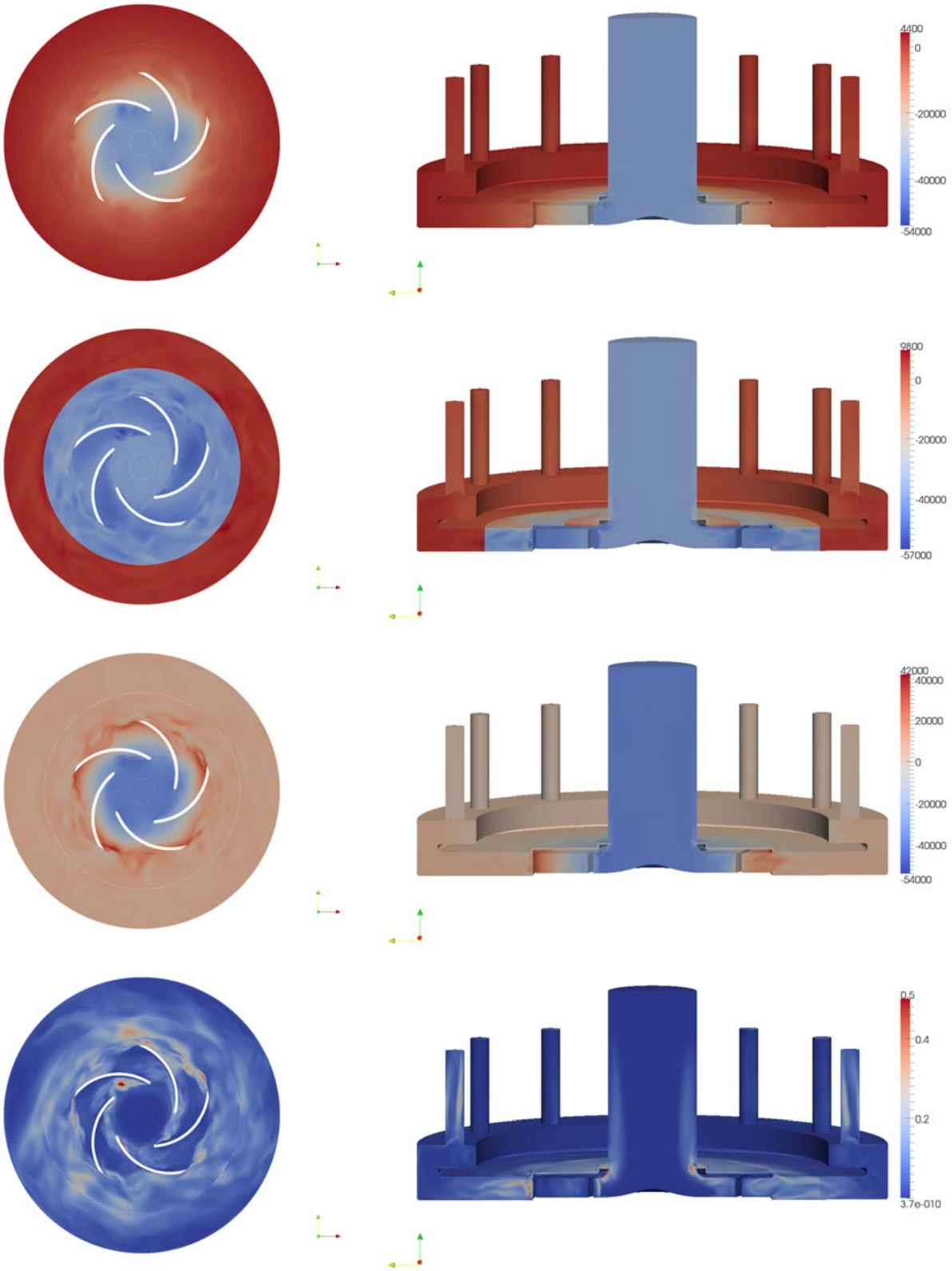

Figure 2: Scalar Values for SAS Model from top to bottom: pressure, total pressure, total pressure in stationary frame, turbulence kinetic energy. The planar slice is located at $z = 0.015$.

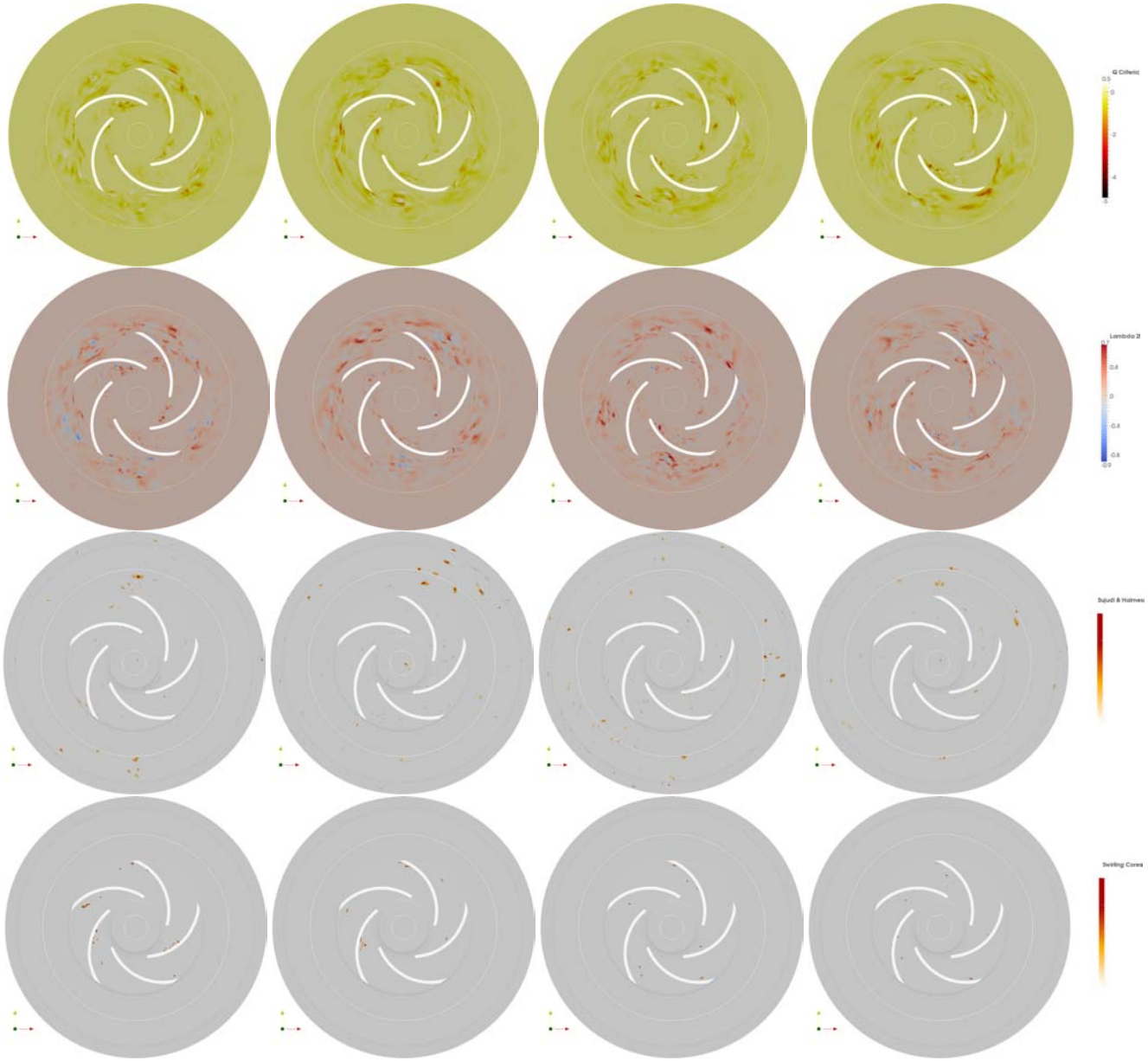

Figure 3: SAS model: Direct comparison of the scalar results of direct vortex criteria for the rotor region for the SAS Model. The slice is located at $z = 0.015$ and every column shows the results for time steps $\tau = 2568, 2668, 2772, 2880$ from left to right. Note, that the last two criteria are displayed by means of a parallel vectors criteria which is a binary decision per cell.

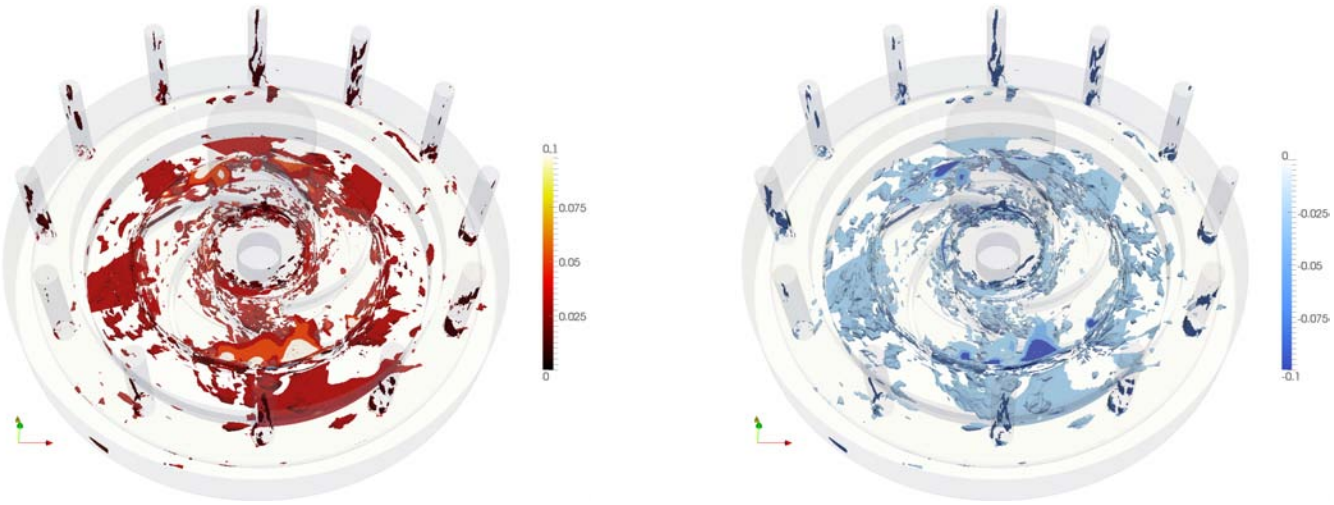

Figure 4: SAS model: Displaying 3D iso surfaces close to zero of all scalar maps. The surfaces reveal additional information about their 3D distribution within the data set. In general the Q and λ_2 criteria detect many smaller vortex regions especially close to boundaries.

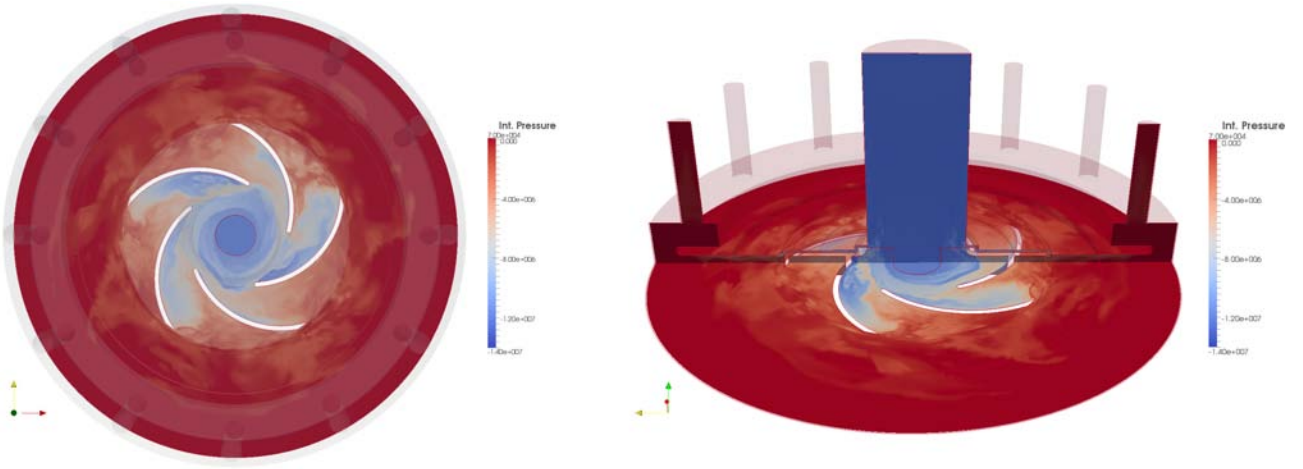

Figure 5: SAS model: Results of direct integral accumulation of the pressure values in forward direction. The images communicate resulting low pressure areas in channel 2, 3 and 5 showing that a large portion of particles would remain in areas with lower pressure.

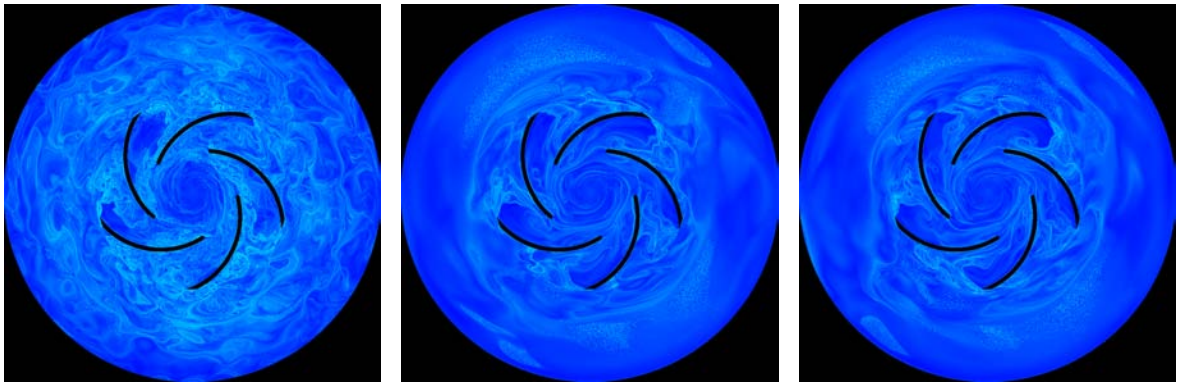

Figure 6: FTLE [3] fields for the SAS, DES and SST (left to right) model for parameters $t_0 = 0, T = 80, z = 0.02$ describing the rate of separation over a fixed time interval. As we used the full available time span to obtain those fields in the SAS model the resulting structures are already very delicate reflecting the high degree of turbulence throughout the dataset. Additionally we used a shorter time span with $T = 20$ in the accompanying video to show the movement of the resulting separation structures. Note, that major ridges in this field can also be observed in the fields of other Lagrangian methods.

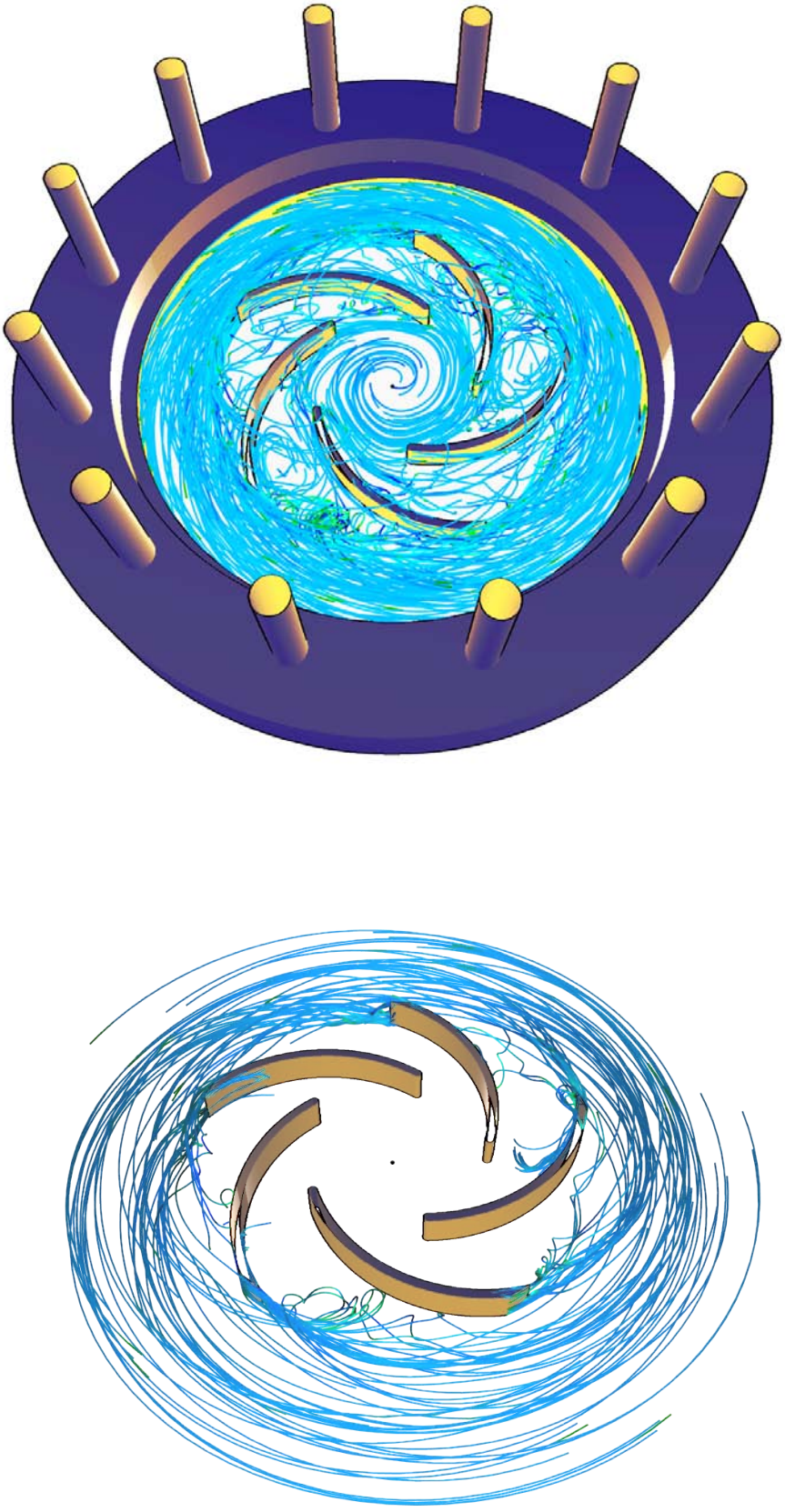

Figure 7: Path lines using SAS model: Path lines provide a basic overview about the flow behavior by illustrating the time-dependent path of *actual* physical massless tracer particles within the flow. These path lines are computed in relative frame of reference turning with the rotor. The first image shows path lines randomly seeded inside the rotor volume. The second image shows path lines seeded at the end of the rotor blades. Dark blue colors indicate path lines flowing downwards, light blue denotes upward flow (in positive Z-direction), green addtionally encodes local curvature of the path lines.

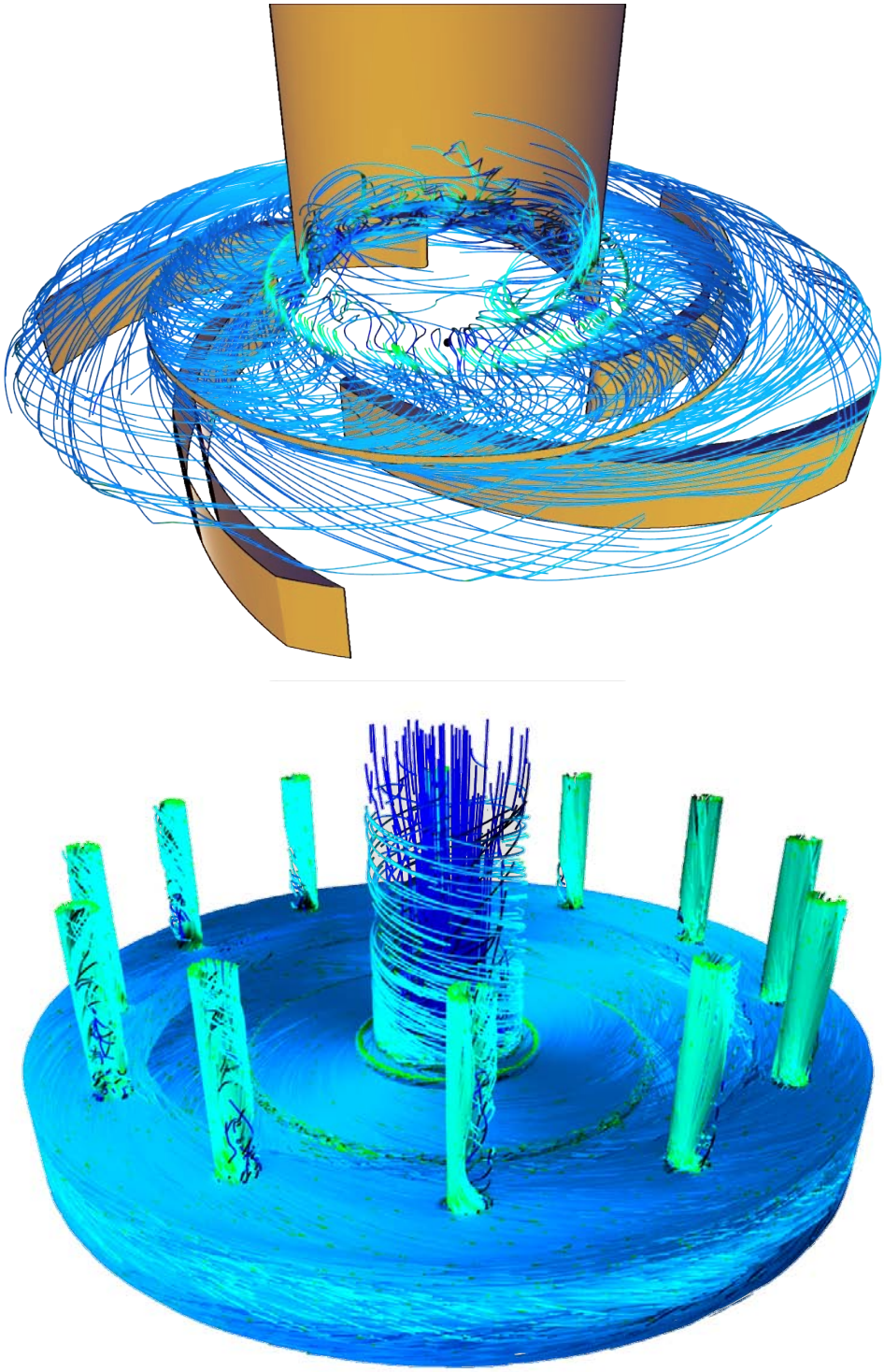

Figure 8: Unsteady particle paths using SAS model: Path lines have the same color coding described in figure 7. The first image shows path lines computed in the relative frame of reference which are seeded at part *Spalt SS side 1 boundary*. The second image contains dense seeded path lines in the absolute frame of reference. In both images we can see particle paths seeded in the inlet region (light blue) indicating movement against the expected flow direction (dark blue). In the second image we also can observe this behavior at the outlets where dark blue particles move against the expected direction.

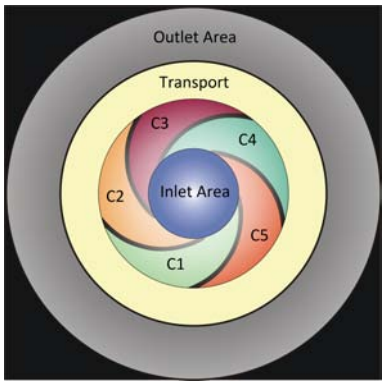

Start Texture

SAS

DES

SST

Figure 9: Advecting structured patterns reveals additional transport information about the flow. We applied an forward advection of a 2D texture projected into the flow volume. In the resulting image we can see in which section one point in the texture would end up after a variable integration time in one slice at $z = 0.02$. The first image shows the original pattern. In rows 2 to 4 this texture is advected to the time steps 26, 52 and 80 for each simulation model. We see the impact of the turbulence and evolving vortical patterns at the section boundaries. These images show clearly the differences between the simulation models. *At time step 26* we see evolving the first vortical structures and also the beginning of the distribution of the inflow of the channels. *At time step 52* it becomes visible that in the SAS the inflow of channels 1 and 4 block the inflow of the other channels, which is not the case using DES an SST. In all three models we can also see that some areas of the outer region move back into the transport area and even into the channels. *At time step 80* the fully evolved transport pattern is shown. The images reveal large recirculation structures behind the rotor blades, especially in channel 3 and 5 of the SAS model.

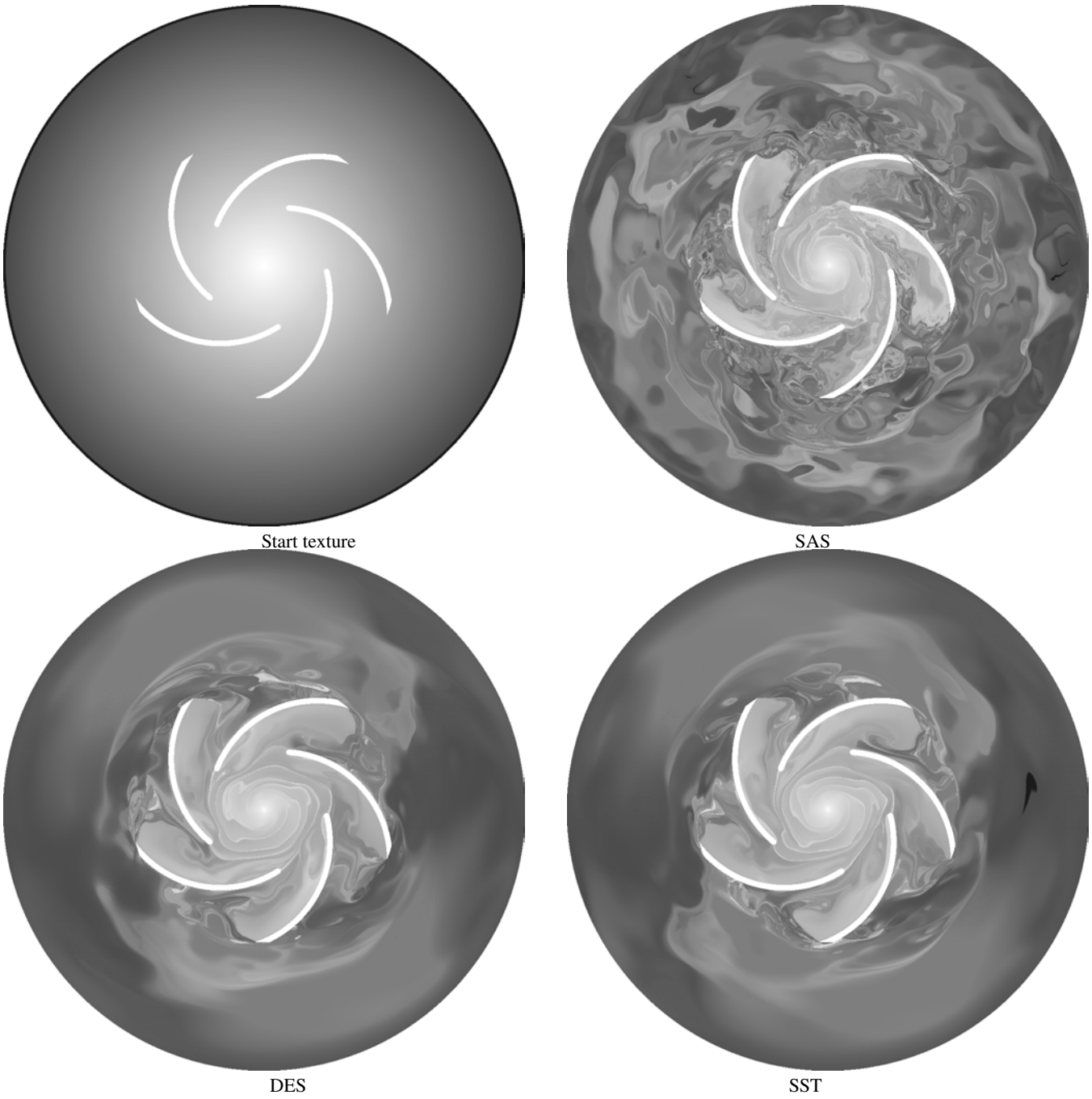

Figure 10: Texture advection of a gradient texture showing the transport behavior form interior to outward regions and additionally internal recirculation areas.

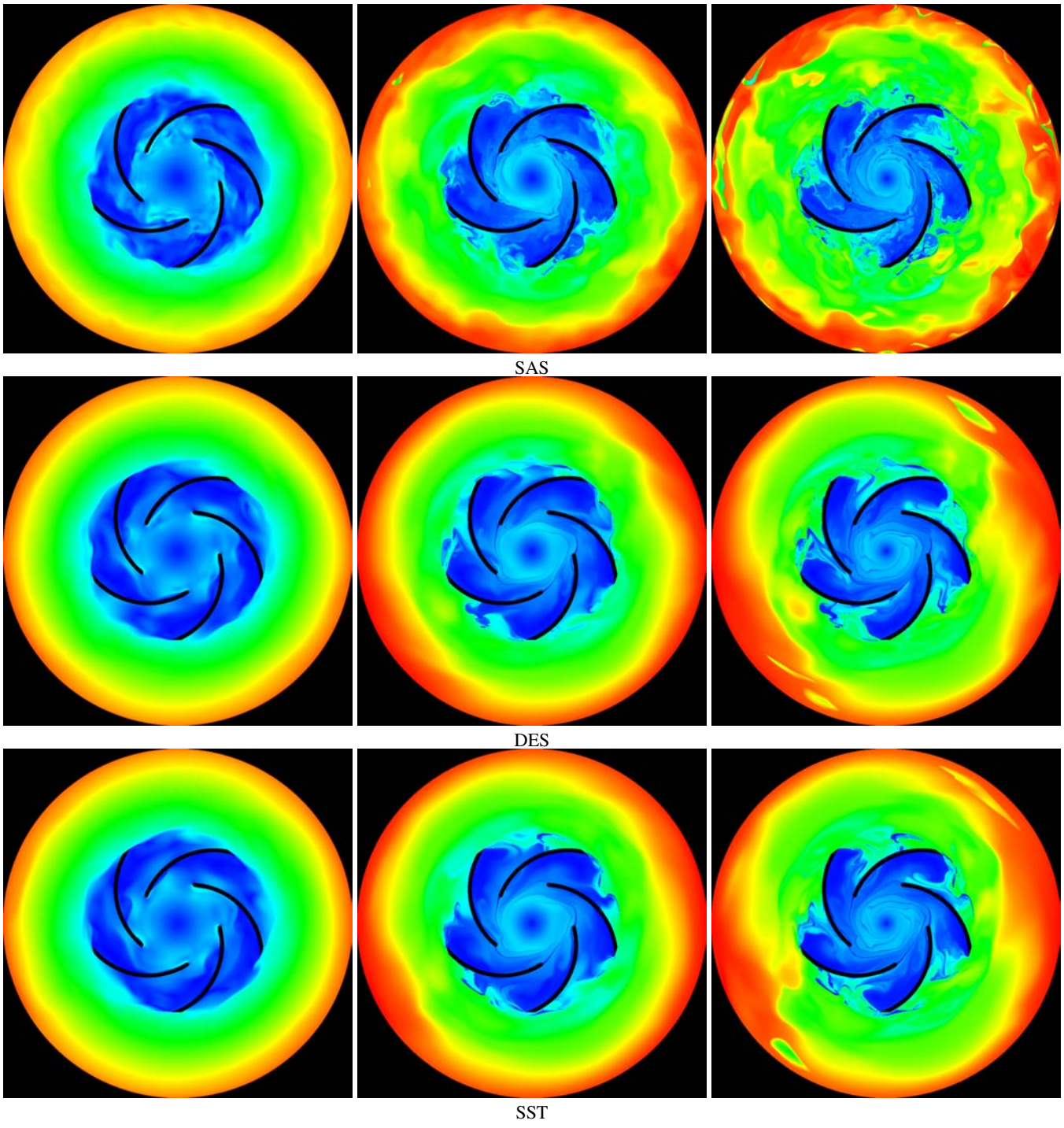

Figure 11: Global integral features as the path line arc length further emphasize regions of special interest. In this length plots red regions can be interpreted as fast moving features over the respective time range shown in one slice at $z = 0.02$ in the relative frame of reference. In this case, slower particles indicate material structures by means of valley structures and hint on vortex regions as small isolated minima. The first column shows the vector length already indicating small vortical structures at the tip of the impeller blades. Column 2 and 3 show the evolution of the path line arc length at time steps 40 and 80.